Evidence of a Double Surface Crossing between Open- and Closed-Shell Surfaces in the Photodissociation of Cyclopropyl Iodide

Pamela A. Arnold,[†] Bogdan R. Cosofret,[†] Scott M. Dylewski,[‡] Paul L. Houston,*[,†] and Barry K. Carpenter*[,†]

Department of Chemistry and Chemical Biology, Cornell University, Ithaca, New York 14853-1301, and School of Applied and Engineering Physics, Cornell University, Ithaca, New York 14853-2501

Received: October 12, 2000; In Final Form: January 8, 2001

Gas-phase photodissociations of cyclopropyl iodide were conducted at 266 and 279.7 nm, and the radical products were probed by multiphoton ionization, with imaging of the resulting ions and their corresponding electrons. Solution-phase photodissociations of cyclopropyl iodide were also conducted with TEMPO-trapping of the radical dissociation products. In both gas and solution phases, allyl radical was found to be a direct product of the cyclopropyl iodide photodissociation. CASSCF calculations indicate that the allyl radical could be formed directly from photoexcited cyclopropyl iodide by way of two surface crossings between open- and closed-shell potential energy surfaces. Each surface crossing represents a point of potential bifurcation in the reaction dynamics. Thus, cyclopropyl iodide that is excited to a $^1(n,\sigma^*)$ state can remain on an open-shell surface and generate the cyclopropyl radical and an iodine atom or can cross to a closed-shell (ion-pair) surface. The cyclopropyl cation that results from the surface crossing can undergo barrierless ring opening to the allyl cation before crossing back to an open-shell surface to generate allyl radical and an iodine atom. In this manner, both cyclopropyl radical and allyl radical can be formed as direct products of cyclopropyl iodide photodissociation.

1. Introduction

Photoinduced homolytic cleavage of alkyl−halogen bonds is a commonly employed method for the generation of alkyl radicals. However, in some instances, solution-phase irradiations of alkyl halides have been found to result in the formation of products that can only be explained by ionic rearrangements of the alkyl fragments.[1] Kropp has explained these observations in terms of an electron-transfer mechanism. He suggests that homolytic dissociation of alkyl halides generates a solvent-caged radical pair, which can, in some cases, undergo electron transfer to generate an ion pair.[1] Presumably there should be no gas-phase counterpart to this reaction.

Recent efforts in our laboratories have focused on the generation of cyclopropyl radical by the photodissociation of cyclopropyl iodide. As described below, the results suggest involvement of an ion pair in *both* gas and solution phases. Cyclopropyl iodide is a particularly suitable substrate for this investigation, as the differing reactivities of cyclopropyl radical and cyclopropyl cation make it possible to distinguish between ionic and radical processes.

The isomerization of cyclopropyl radical to allyl radical has been the subject of many computational efforts[2−8] but few experimental studies. Experimentally determined activation enthalpies for the ring opening of cyclopropyl radical range from 19.1 to 22 kcal/mol.[9−11] Computationally determined values for the enthalpy barrier are in close agreement with the experimental values.[8,12]

The reaction enthalpy for the cyclopropyl radical ring opening is not well-established. On the basis of experimental determinations of the heats of formation of allyl radical and cyclopropyl radical, the enthalpy for ring opening has been determined to be between −22.8 and −25.6 kcal/mol.[13,14] However, computational studies consistently show the reaction enthalpy to be approximately −32 kcal/mol.[8,12] Whether the error in the values for the enthalpy of ring opening lies in the experimental measurements, in the calculations, or in both is unclear.

Presumably due to the high activation energy, isomerization to allyl radical has only been observed to occur from vibrationally excited cyclopropyl radical in the gas phase.[15,16] Despite the highly exothermic nature of the ring opening, it has not been reported to occur in solution.

Cyclopropyl cation, on the other hand, can undergo isomerization to allyl cation with little to no energy barrier and an enthalpy change of approximately −30 to −36 kcal/mol.[12,17] This difference in reactivity between the cyclopropyl radical and the cyclopropyl cation makes it possible to differentiate between radical and ionic pathways under specific reaction conditions.

On the basis of the experimental results and ab initio calculations reported herein, we propose a mechanism for the photodissociation of cyclopropyl iodide involving two intersections between open- and closed-shell potential energy surfaces (PES). The first intersection provides a means by which the closely associated cyclopropyl radical and iodine atom cross from the open-shell (radical-pair) to the closed-shell (ion-pair) PES. The resulting cyclopropyl cation can then undergo barrierless ring opening to generate allyl cation, still closely associated with iodine anion. A second intersection between this closed-shell surface and the open-shell surface for allyl iodide dissociation allows allyl radical and an iodine atom to be formed.

* To whom correspondence should be addressed.
[†] Department of Chemistry and Chemical Biology.
[‡] School of Applied and Engineering Physics.

10.1021/jp0037504 CCC: $20.00
Published on Web 02/13/2001

The apparent detection of PES intersections in the photodissociation of cyclopropyl iodide and the reported examples of ionic rearrangements in alkyl halide photodissociations lead us to believe that conical intersections may be prevalent in alkyl halide photodissociations.

2. Experimental Section

2.1. Synthesis of Cyclopropyl Iodide. A 1-L, three-necked, round-bottomed flask was equipped with a stir bar, a reflux condenser, and a 500-mL addition funnel. Magnesium turnings (3.83 g, 0.16 mol), a crystal of I_2, and 50 mL of ether were added to the reaction flask, and a solution of 1-bromocyclopropane (12.0 mL, 0.15 mol) in 350 mL of ether was added to the addition funnel. Approximately 50 mL of the 1-bromocyclopropane solution was added to the magnesium turnings, and the mixture was refluxed with stirring until the brown color from the iodine disappeared. The remainder of the 1-bromocyclopropane solution was then added dropwise, with refluxing and vigorous stirring over a period of 4 h. Reflux was continued for 1 h, then the reaction flask was cooled in an ice bath. To the chilled mixture of cyclopropylmagnesium bromide was added I_2 (41 g, 0.16 mol) gradually via a solid addition funnel. The reaction was allowed to warm to room temperature while stirring was continued for 1.5 h.

The reaction was quenched by slow addition of 2 N HCl. The layers were separated, and the organic layer was washed five times with aqueous saturated sodium thiosulfate, one time with aqueous saturated sodium bicarbonate, and one time with aqueous saturated sodium chloride. The organic layer was then dried over magnesium sulfate and filtered. Ether was removed by distillation at atmospheric pressure.

Cyclopropyl iodide was isolated from the product mixture by flash column chromatography, eluting with 100% pentane. Fractions containing 97−99% cyclopropyl iodide, as determined by gas chromatography, were combined and pentane was removed by distillation at atmospheric pressure. The remaining oil was then fractionally distilled at atmospheric pressure. The fraction boiling at 95−100 °C contained 99% cyclopropyl iodide (3.63 g, 14% yield). The product is a colorless oil.

2.2. Solution-Phase Photodissociation of Cyclopropyl Iodide. Two separate 0.0536 M solutions of cyclopropyl iodide (22.6 mg, 0.134 mmol) in benzene (2.5 mL) were irradiated with an Ace-Hanovia 450-W medium-pressure mercury-vapor lamp for 50 h, at 9.7 °C, in the presence of a large excess of 2,2,6,6-tetramethyl-1-piperidinyloxy (TEMPO) radical trap. One solution contained 2.46 M TEMPO (0.962 g, 6.15 mmol) and the other solution contained 1.28 M TEMPO (0.500 g, 3.20 mmol). The reaction progress and the change in product ratios over time were monitored by gas chromatography. The reaction products were characterized by NMR and GC/MS. The isolated TEMPO-trapped products were shown through independent irradiation to be stable under the reaction conditions.

2.3. Gas-Phase Photodissociation of Cyclopropyl Iodide. The gas-phase photodissociation of cyclopropyl iodide was investigated using ion imaging and electron imaging techniques. The technique of ion imaging has been described in more detail elsewhere.[18,19] Alkyl iodides were introduced into the chamber by bubbling He through the samples, which were cooled in ice and acetone at −10 °C. The mixture was expanded at 17 psi through a pulsed 250 μm diameter nozzle and collimated by a 500 μm diameter skimmer mounted 0.5−1 cm from the nozzle orifice. Further downstream, the molecular beam was crossed at right angles by two counterpropagating laser beams, one used to dissociate the alkyl iodide and the other to probe the resulting $I(^2P_{1/2})$ and $I(^2P_{3/2})$ fragments using the 2 + 1 resonance-enhanced multiphoton ionization (REMPI) schemes at 304.0 nm ($5p\ ^3P_{0,1,2}$, $^1D_2 \leftarrow 5p\ ^2P_{1/2}$) and 304.6 nm ($5p\ ^3P_2 \leftarrow 5p\ ^2P_{3/2}$), respectively. Due to the large Doppler width of the $I(^2P_{1/2})$ and $I(^2P_{3/2})$ fragments it was necessary to scan the probe laser over the resonance to ensure that the images detected all iodine atom velocities with equal sensitivity.

The dissociation laser radiation at 266 nm was produced by doubling the 532 nm output from a Nd:YAG laser using an 83° KDP crystal. Typical powers obtained were about 20 mJ/pulse with a pulse duration of 8−10 ns. The tunable light needed to probe the $I(^2P_{1/2})$ and $I(^2P_{3/2})$ fragments at 304.0 and 304.6 nm, respectively, was generated by frequency doubling the output of an injection-seeded, Nd:YAG−pumped dye laser; typical powers achieved were 2.0 mJ/pulse with a pulse width of 8−10 ns. The dissociation and the probe beams were directed into the vacuum chamber and focused into the interaction region by 25 and 7.5 cm focal length planoconvex lenses, respectively. The polarizations of both laser beams were perpendicular to the plane defined by the molecular and laser beams. The delay time between the pump and probe lasers was set to 17 ns.

The imaging technique uses an electrostatic immersion lens which serves to extract the ionized fragments $I(^2P_{1/2})$ and $I(^2P_{3/2})$ from the interaction region and to focus ions with equal velocity vectors to the same point on the detector.[20] The magnification factor of this electrostatic lens was measured to be 1.17 ± 0.03 by dissociating O_2 at 225.65 nm and detecting the $O(^3P_2)$ fragment using the $O(3p\ ^3P_{2,1,0} \leftarrow 2p\ ^3P_2)$ 2+1 REMPI scheme.

The ionized fragments were accelerated into a field-free flight tube mounted along the axis of the molecular beam. The ions were imaged using a position sensitive detector consisting of a chevron double microchannel plate (MCP) assembly coupled to a fast phosphor screen. The image on the screen was recorded with a 640 × 480 pixel CCD camera. Both the MCP and the camera were electronically gated to collect signal corresponding only to the mass of the $I(^2P_{1/2})$ and $I(^2P_{3/2})$ fragments. Signal levels were kept below 300 ions per frame to avoid saturation of the MCP. Data were accumulated typically for 80 000 total laser shots.

The experimental setup was slightly modified for electron imaging. Both the electrostatic lens and the flight tube were carefully wrapped in a grounded sheet of μ-metal to provide magnetic shielding. The original time-of-flight (TOF) tube, which produced a TOF distance of 62.5 cm, was replaced by a shorter tube with a TOF distance of 41.5 cm to compensate for the greater velocity of electrons. This modification allowed the entire electron signal to be focused on the detector. In the electron-imaging experiments, only one laser was used for both dissociation and ionization, and the experiments were conducted in two separate wavelength regions. The radiation in the 266-nm region was obtained in the same manner as described above, while the laser light radiation in the region between 279 and 285 nm was obtained by frequency doubling the output of an injection-seeded Nd:YAG−pumped dye laser using a 74° KDP crystal. Typical powers for both regions were kept at low values between 2 and 3 mJ/pulse to avoid nonresonant interactions.

Due to the large velocities of electrons, their TOF is very short and arrival at the detection source is almost instantaneous. Thus, to detect electrons, it was necessary to electronically gate the MCP and the camera for the duration of the laser pulse.

Due to these modifications to the apparatus for electron imaging, new calibrations were needed for the magnification factor and electron time-of-flight. These calibrations were achieved by carrying out state-selected ionizations of atomic

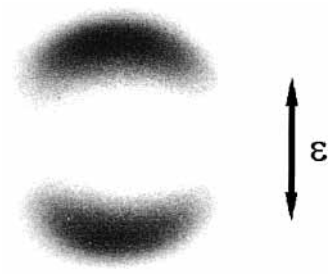

Figure 1. Raw iodine image from the 266-nm dissociation of cyclopropyl iodide followed by 304.6-nm ($5p\ ^3P_2 \leftarrow 5p\ ^2P_{3/2}$) ionization of iodine. The polarization of the dissociation light was parallel to the vertical direction of the figure.

iodine at 280.99, 280.69, 281.73, and 279.71 nm to produce electrons with known energies. Jung et al. have published the 2 + 1 REMPI lines of atomic iodine between 277 and 313 nm and their branching ratios to the various available states of I^+.[21] These branching ratios and the energies of the I^+ states published by Wang et al.[22] were used to calculate the energies of the electrons from ionization of iodine. The electron time-of-flight and magnification factor were then calibrated by adjusting their values so that the experimentally obtained energy distributions coincided with the known electron energies. These calibrated values were then used in the processing of all electron images. Calibration images were collected periodically to confirm that the calibrations remained constant.

2.4. Computational Methods. Calculations were carried out using Gaussian 98[23] on a 500-MHz dual-processor Compaq DS20E workstation and using GAMESS[24] on a 466-MHz G3 Macintosh. Conical intersections were located by use of the routine incorporated in Gaussian 98.[25] Orbitals were visualized using MacMolPlt[26] and GaussView 2.0.

3. Results

3.1. Gas-Phase Photodissociation of Cyclopropyl Iodide. The radical fragments generated from a photodissociation process scatter from the center of mass in three dimensions. The velocities of the fragments relative to the center of mass are proportional to the square root of their kinetic energies. When these fragments are ionized and then accelerated to the detector, the image that is observed is a two-dimensional projection of the three-dimensional distribution of ions onto the plane of the detector, such as shown in Figure 1. The intensity at each pixel is proportional to the number of ions detected at that position. The three-dimensional velocity distribution of the fragments relative to the center of mass is reconstructed from the two-dimensional image by taking the inverse Abel transform of the symmetrized raw image.[27,28] The angular, speed, and kinetic energy distributions of the fragments (also relative to the center of mass) are then derived from the reconstructed three-dimensional distribution.

3.1.1. Ion Imaging. The total kinetic energy distribution of the radical fragments that were formed from dissociation of cyclopropyl iodide at 266 nm was determined using ion imaging techniques. The 266 nm dissociation of cyclopropyl iodide was found to generate iodine radicals in both the $^2P_{3/2}$ and $^2P_{1/2}$ spin−orbit states, which were ionized at 304.6 and 304.0 nm, respectively. Figure 1 shows the raw image from the 304.6 nm ($5p\ ^3P_2 \leftarrow 5p\ ^2P_{3/2}$) ionization of iodine. The relative kinetic energy distributions of the iodine fragments were then determined from the observed relative velocity distributions of the iodine ions, and the kinetic energy distributions of the corresponding alkyl fragments were determined on the basis of conservation of momentum. The total relative kinetic energy distributions of the iodine and alkyl radical fragments formed upon 266-nm dissociation of cyclopropyl iodide are shown in Figure 2.

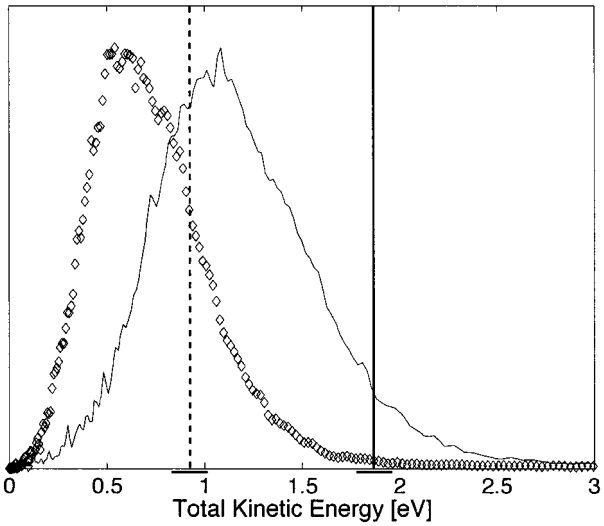

Figure 2. Total relative translational kinetic energy distributions of fragments from 266-nm photodissociations of cyclopropyl iodide, probing the 304.6-nm ($5p\ ^3P_2 \leftarrow 5p\ ^2P_{3/2}$) REMPI transition of atomic iodine (—) and probing the 304.0-nm ($5p\ ^3P_{0,1,2}$, $^1D_2 \leftarrow 5p\ ^2P_{1/2}$) REMPI transition of atomic iodine (◇). The maximum possible kinetic energy, assuming dissociation to cyclopropyl radical and an iodine atom, is denoted by the vertical lines. The solid line at 1.87 eV is the maximum KE for formation of $I\ ^2P_{3/2}$ and the dashed line at 0.93 eV is the maximum KE for formation of $I\ ^2P_{1/2}$. Horizontal error bars representing the 0.09 eV uncertainty in the maximum kinetic energy are shown just below the KE axis of the graph.

The anisotropy of the angular distribution is described by the parameter β in $I(\theta) \propto [1 + \beta P_2(\cos\theta)]$, where θ is the angle between the electric vector of the dissociation light and the recoil direction and $P_2(\cos\theta)$ is the second Legendre polynomial. Fits to the data reveal that $\beta = 1.88 \pm 0.27$ for the channel producing the ground state of the I atom and $\beta = 1.91 \pm 0.12$ for the channel producing the spin−orbit excited state of I.

3.1.2. Electron Imaging. Photodissociations of cyclopropyl iodide and allyl iodide and ionizations of the resulting fragments were independently carried out at both 266 and 279.7 nm. The electron energy distributions resulting from the 266 nm dissociations and ionizations are shown in Figure 3. It can be seen that three distinct populations of electrons at 0.18 eV (A), 1.0 eV (B), and 2.4 eV (C) are generated from *both* the cyclopropyl iodide and the allyl iodide experiments.

These energy distributions were obtained by dissociating and ionizing near the center of the molecular beam profile, where the density of molecules is at its greatest and formation and ionization of clusters is highly probable. It is notable that when the dissociations and ionizations were carried out at the more dilute front edge of the molecular beam, populations A and C dramatically decreased relative to B. Additionally, upon photodissociation and ionization of methyl iodide under the same experimental conditions and near the center of the molecular beam, populations A and C were again observed, but B was not. From this it was concluded that populations A and C were from ionization of clusters, whereas B was from the ionization of a common product formed from both the allyl iodide and cyclopropyl iodide dissociations.

When dissociations of cyclopropyl iodide and allyl iodide and ionizations of the resulting alkyl fragments were carried

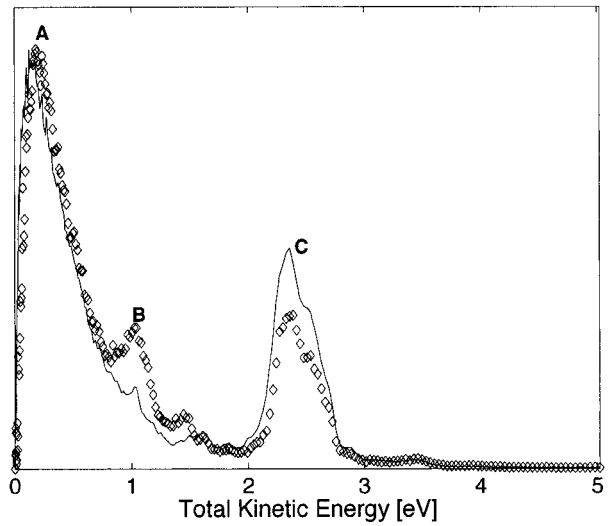

Figure 3. Electron energy distributions from 266 nm ionizations of allyl iodide (◇) and cyclopropyl iodide (_) photodissociation products. Three distinct populations of electrons were observed at 0.18 eV (A), 1.0 eV (B) and 2.4 eV (C).

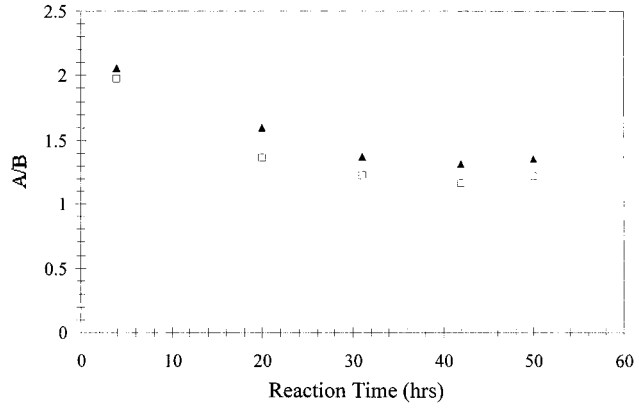

Figure 4. Ratio of products cyclopropyl 2,2,6,6-tetramethyl-piperidin-1-yl ester (A) and allyl 2,2,6,6-tetramethyl-piperidin-1-yl ester (B) as a function of time and concentration of TEMPO radical trap: (▲) 2.46 M TEMPO and (□) 1.28 M TEMPO.

out at 279.7 nm, coinciding electron distributions were again detected, in this case at 0.80 eV. This result is again consistent with the formation of a common product from both allyl iodide and cyclopropyl iodide dissociations.

3.2. Solution-Phase Photodissociation of Cyclopropyl Iodide. The TEMPO-trapped products of solution-phase photodissociation of cyclopropyl iodide were determined to be cyclopropyl 2,2,6,6-tetramethyl-piperidin-1-yl ester (A) and allyl 2,2,6,6-tetramethyl-piperidin-1-yl ester (B), as well as cyclopropyl iodide and allyl iodide. A plot of the ratio of products A to B as a function of time and TEMPO concentration is shown in Figure 4.

4. Discussion

The gas and solution-phase results suggest that allyl radical is formed as a direct product of cyclopropyl iodide photodissociation. In the sections 4.1 through 4.4 we will provide a detailed discussion of our interpretation of the results from each experiment and thereby explain how this conclusion was reached. Further details on a possible mechanism for the formation of allyl radical from cyclopropyl iodide photodissociation were obtained through ab initio calculations. These will be discussed in sections 4.5 and 4.6.

4.1. Gas-Phase Ion Imaging. It was expected that the gas-phase photodissociation of cyclopropyl iodide at 266 nm would result in the formation of iodine atoms and vibrationally excited cyclopropyl radicals. It should then be possible to determine the internal energy distribution of the cyclopropyl radicals using eq 1:

$$E_{\text{int}} = h\upsilon - \text{BDE} - \text{KE}_{\text{tot}} \quad (1)$$

In eq 1, E_{int} is the internal energy of the cyclopropyl fragments, $h\upsilon$ is the energy of the dissociating light, and BDE is the C−I bond dissociation enthalpy of cyclopropyl iodide. KE_{tot} is the total relative kinetic energy of the cyclopropyl fragments and the iodine atoms, determined as previously described.

*4.1.1. Estimation of C−I Bond Dissociation Enthalpy.*To our knowledge, there are no direct experimental determinations of the C−I bond dissociation enthalpy (BDE) of cyclopropyl iodide. There is one estimate of 58.6 kcal/mol in the literature,[29] but this is based on a value of $\Delta H_f^\circ = 61.3$ kcal/mol for the cyclopropyl radical, which was deduced by studying the kinetics of hydrogen atom abstraction from cyclopropane.[30] More recent measurements, based on the gas-phase acidity of cyclopropane[31] and the electron affinity of the cyclopropyl radical,[32] bring the heat of formation up to 67.7 kcal/mol. This correction would raise the estimated[29] BDE to 65.0 kcal/mol.

An alternative estimate of the C−I BDE can come from assuming that the hypothetical reaction shown in eq 2 is thermoneutral:

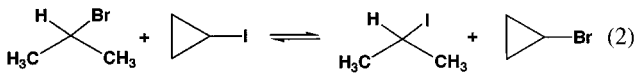

(2)

With that assumption, one can use the experimental BDEs of isopropyl bromide,[33] isopropyl iodide,[34] and cyclopropyl bromide[35] to estimate the desired quantity. The value turns out to be 64.0 kcal/mol.

As independent estimates, we have also carried out ab initio calculations on the isodesmic reactions shown in eqs 3 and 4:

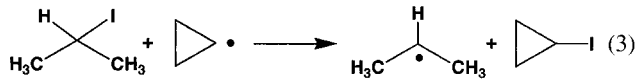

(3)

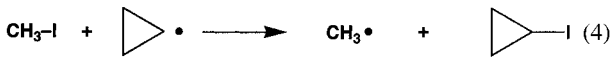

(4)

The calculations were carried out at the (U)MP2 level and used a 3-21G* basis set on iodine and a 6-31G* basis set on the hydrocarbon radicals. The calculated ΔH° values for eqs 3 and 4 were respectively −7.51 and −10.02 kcal/mol. These values, in combination with the experimental C−I BDEs of isopropyl iodide[34] and methyl iodide,[36] give values of respectively 62.4 and 66.9 kcal/mol for the C−I BDE of cyclopropyl iodide.

In summary, the four independent estimates of the C−I BDE of cyclopropyl iodide give a value of 64.5 ± 2 kcal/mol. Following the normal convention, this estimate of the BDE refers to the formation of the fragments in their ground states. However, in the gas-phase photodissociations we were able to detect the iodine atom both in its ground $^2P_{3/2}$ (which we will call the I channel) state and in the spin−orbit excited $^2P_{1/2}$ state (the I* channel). It is consequently convenient to define a second BDE for this latter event. Its value, 86.2 ± 2 kcal/mol, differs from the ground-state value by an amount equal to the energy difference (7603 cm^{-1}) between the two iodine-atom spin−orbit states.

4.1.2. Determination of E_{int}: Evidence of an Alternative Dissociation Mechanism. Using eq 1 and the value of 64.5 ± 2 kcal/mol (2.79 ± 0.09 eV) for the C−I BDE, a maximum possible total kinetic energy is calculated to be 1.87 ± 0.09 eV when dissociation to cyclopropyl radical and I $^2P_{3/2}$ is carried out at 266 nm. This maximum energy would be achieved in the improbable event that E_{int} were equal to zero or, in other words, if the cyclopropyl radical were generated with no vibrational or rotational energy. For dissociation to cyclopropyl radical and I $^2P_{1/2}$, the maximum translational KE would be 0.93 ± 0.09 eV. It is noteworthy that significant fractions of the fragments exceed these maximum values in both the I and I* channels, as shown in Figure 2. This result would imply that some of the cyclopropyl radicals are generated with negative internal energy! Thus, we are led to conclude that the radical fragments of higher kinetic energy are generated from an alternative dissociation process with a lower BDE. A direct dissociation of cyclopropyl iodide into allyl radical and iodine seems the most likely alternative. Adding the computed 1.39 eV exothermicity for ring opening of cyclopropyl to allyl radical[8,12] to the maximum translational KE values would shift the vertical lines in Figure 2 up to 3.26 eV for the I channel and 2.32 eV for the I* channel. The data reveal that none of the experimental kinetic energies exceed these revised limits.

4.2. Detection of Allyl Radical by Electron Imaging. To determine whether allyl radical was formed from the gas-phase photodissociation of cyclopropyl iodide, we ionized the alkyl fragments and imaged the resulting electrons. The results of these electron imaging experiments, shown in Figure 3, indicate that a common product is formed from the independent photodissociations of cyclopropyl iodide and allyl iodide. To test our postulate that this common product is the allyl radical, we have calculated the approximate values for the electron kinetic energies formed from ionization of allyl radical at 266 and 279.7 nm and compared these values to the observed electron kinetic energies. The calculated values come from eq 5, in which KE is the kinetic energy of the electrons, $h\nu$ is the total energy of the photons absorbed, and IP is the vertical ionization potential for the allyl radical.

$$\mathrm{KE} = h\nu - \mathrm{IP} \tag{5}$$

The vertical and adiabatic ionization energies of allyl radical have experimentally been found to coincide at 8.13 eV,[37,38] indicating similar equilibrium geometries for the allyl radical and cation. Although the allyl radicals produced in the photodissociation of allyl iodide are vibrationally excited, because of the similar geometries for the radical and cation, it is likely that the Franck−Condon factors governing the ionization will favor transitions to similarly vibrationally excited states of the cation. Therefore, we presume that ionization of the allyl radical generated in these studies would require approximately 8.13 eV. On the basis of this value, the energy of electrons from 1 + 1 REMPI ionizations of allyl radical at 266 and 279.7 nm are calculated to be approximately 1.19 and 0.73 eV, respectively. The agreement between the expected values for electron energies and the experimentally observed electron populations at 1.0 and 0.80 eV provides support for the postulate that allyl radical is the common product to which these electrons can be assigned.

4.3. RRKM Calculations on the Ring Opening of Cyclopropyl Radical. While allyl radical does, indeed, appear to be formed from the photodissociation of cyclopropyl iodide within the 8−10 ns time scale of the experiments, the question of how it is formed still remains. The ion imaging results point toward the existence of a mechanism by which cyclopropyl iodide dissociates directly to allyl radical. However, the radical fragments with lower kinetic energy (thus, higher internal energy) may well come from the simple homolytic dissociation of cyclopropyl iodide to form cyclopropyl radical and an iodine atom. If such is the case, then these vibrationally excited cyclopropyl radicals could also generate allyl radical by subsequent ring opening.

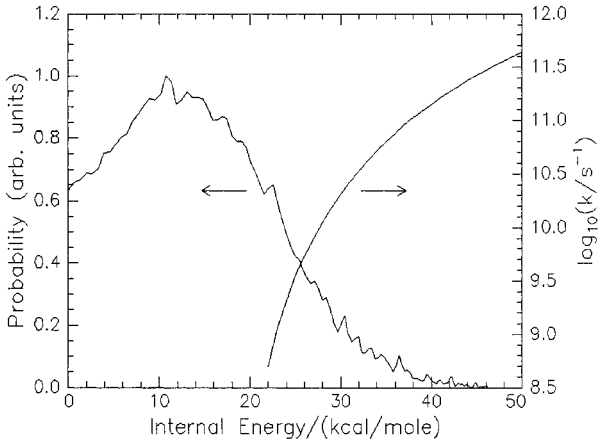

Figure 5. RRKM-determined rate constants for the gas-phase ring opening of cyclopropyl radical plotted as a function of the internal energy of the cyclopropyl radical (right curve). Internal energy distribution of alkyl fragments formed from photodissociation of cyclopropyl iodide in the I channel (left curve).

TABLE 1: Input Parameters Used for the RRKM Calculation of the Cyclopropyl Radical Ring Opening[a]

cyclopropyl radical	
relative energy	[0]
no. of oscillators	18
no. of internal rotors	0
frequencies (cm^{-1})	697.0, 815.0, 840.0, 849.0, 999.0, 1130.0, 1169.0, 1187.0, 1216.0, 1229.0, 1300.0, 1572.0, 1608.0, 3239.0, 3245.0, 3312.0, 3324.0, 3355.0
transition state between cyclopropyl radical and allyl radical	
relative energy (kcal/mol)	21.0
no. of oscillators	17
no. of internal rotors	0
frequencies (cm^{-1})	464.0, 590.0, 659.0, 793.0, 879.0, 944.0, 1140.0, 1176.0, 1300.0, 1408.0, 1561.0, 1614.0, 3251.0, 3286.0, 3310.0, 3359.0, 3391.0
moments of inertia (amu·Å^2)	16.19, 36.34, 46.09
moments of inertia (amu·Å^2)	20.94, 24.60, 38.19

[a] Parameters were determined from CASPT2(3,3)/cc-pVTZ//CASSCF(3,3)/cc-pVTZ calculations.[12]

Approximate rate constants for the ring opening of cyclopropyl radical as a function of the internal energy of the cyclopropyl radical have been calculated using RRKM theory[39] and are plotted in Figure 5. The structures, energies, frequencies, and moments of inertia of the cyclopropyl radical and the transition state to allyl radical were calculated at the CASPT2(3,3)/cc-pVTZ//CASSCF(3,3)/cc-pVTZ level[12] and are listed in Table 1.

The observed internal energy distribution of the alkyl fragments formed in the I channel following 266 nm dissociation of cyclopropyl iodide is also shown in Figure 5. It can be seen that the cyclopropyl radicals with internal energy of 22 kcal/mol can ring open on a time scale of approximately 2 ns, while

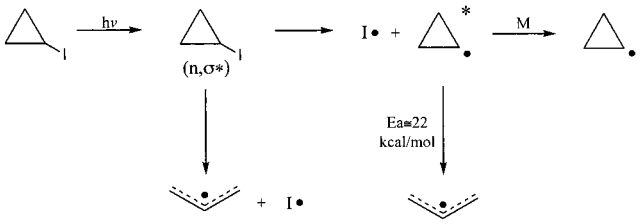

Figure 6. Two mechanisms for the formation of allyl radical from cyclopropyl iodide photodissociation: (1) direct formation from the (n,σ^*) photoexcited state of cyclopropyl iodide and (2) ring opening of vibrationally excited cyclopropyl radical, denoted by asterisk, in competition with vibrational cooling by collision partner M.

those with an internal energy of 30 kcal/mol can ring open on a time scale of approximately 70 ps.

It can be concluded that the experimentally observed allyl radical could be formed from the ring opening of vibrationally excited cyclopropyl radical, and it could also be formed from the direct photodissociation of cyclopropyl iodide in the gas phase. These two pathways for formation of allyl radical are depicted in Figure 6. Since the former process is estimated to occur on the order of picoseconds to nanoseconds, while the latter could occur on a femtosecond time scale, the availability of femtosecond time-resolved electron imaging could provide further insight into the origin of the allyl radical. Such experiments have not been carried out at this time.

4.4. Solution-Phase Photodissociation of Cyclopropyl Iodide. The solution-phase photodissociation of cyclopropyl iodide was expected to produce cyclopropyl radical, which would then be trapped by TEMPO with a rate constant on the order of 10^9 M^{-1} s^{-1}.[40] With an enthalpic barrier of approximately 22 kcal/mol, the thermal ring opening of cyclopropyl radical is unlikely, since collisional cooling (see Figure 6) of any vibrationally hot radicals should be 4−5 orders of magnitude faster than the ring opening. To our knowledge, ring opening of cyclopropyl radical has not been observed in solution phase.

However, upon solution-phase photodissociation of cyclopropyl iodide, TEMPO-trapped products from both allyl and cyclopropyl radicals were found. As shown in Figure 4, the product ratio was found to be only slightly dependent on the concentration of TEMPO. If ring opening were occurring in competition with TEMPO-trapping of the cyclopropyl radical, then doubling the concentration of TEMPO should double the ratio of TEMPO-trapped cyclopropyl radical to TEMPO-trapped allyl radical. The observed product ratio showed a small dependence on the concentration of TEMPO, but not this expected first-order dependence. These results suggest that allyl radical is formed as a direct product from dissociation of photoexcited cyclopropyl iodide.

A slight time dependence was observed in the ratio of products. While this phenomenon has not been investigated in detail, it can be explained by recombination of C_3H_5 radicals and iodine atoms (probably from solvent-caged pairs) to give products that are susceptible to further photolysis. This process would lead to increasing concentrations of allyl iodide in the starting material and hence decreasing ratios of cyclopropyl to allyl TEMPO adducts. The viability of this explanation was demonstrated by the direct observation of allyl iodide in the TEMPO-trapping experiments as well as by an independent experiment showing that cyclopropyl iodide could be converted to allyl iodide when photolyzed in absence of TEMPO.

4.5. Electronic Excited States of Cyclopropyl Iodide. Information about the nature of the initially formed photoexcited state of cyclopropyl iodide is gained from the iodine image shown in Figure 1. The near $\cos^2\theta$ dependence of the recoil velocity distribution on the electric vector of the dissociation light is indicative of a parallel transition. Since excitation occurs from an A′ state and the transition is parallel, the initially formed photoexcited state must also be of A′ symmetry.

In an effort to determine the nature of the electronic excited-state accessed by the 266 nm photolysis, we carried out a CIS calculation on the MP2-optimized geometry of cyclopropyl iodide, using the basis set described earlier. Five singlet electronic excited states were calculated. The results are summarized in Table 2. The orbitals cited in this table are depicted in Figure 7.

The calculations suggest that the longest wavelength absorption of cyclopropyl iodide corresponds to a nominally forbidden transition from the *A*″ p-type lone pair of iodine to the σ_{C-I}* orbital. Promotion of an electron from the *A*′ p-type lone pair to σ_{C-I}* is predicted to be of somewhat higher energy. However, given that the iodine image in Figure 1 shows that the state accessed experimentally is of A′ symmetry, it is likely that these two electronic states are really reversed in relative energy. This disagreement, as well as the fact that the predicted absorption maximum of 212.3 nm does not agree very well with the experimental value of 261 nm (measured in pentane solution), are discrepancies of a magnitude that is common for CIS calculations, which provide only the most rudimentary description of electronic excited states.[41] However, the results probably are reliable enough to conclude that the allowed (σ,σ*) transition of the C−I bond would not be accessible with the 266-nm light used in the experiment.

TABLE 2: Calculated Electronic Transitions of Cyclopropyl Iodide

principal configuration	state symmetry	vertical excitation wavelength (nm)	oscillator strength
38 → 39	A″	222.6	0.0043
37 → 39	A′	212.3	0.0046
36 → 39	A′	144.1	0.5665
35 → 39	A″	143.8	0.0051
34 → 39	A′	127.0	0.2841

[a] Principal configurations of each excited state are defined by transitions from the ground state. The numbers in column 1 refer to the orbitals depicted in Figure 7.

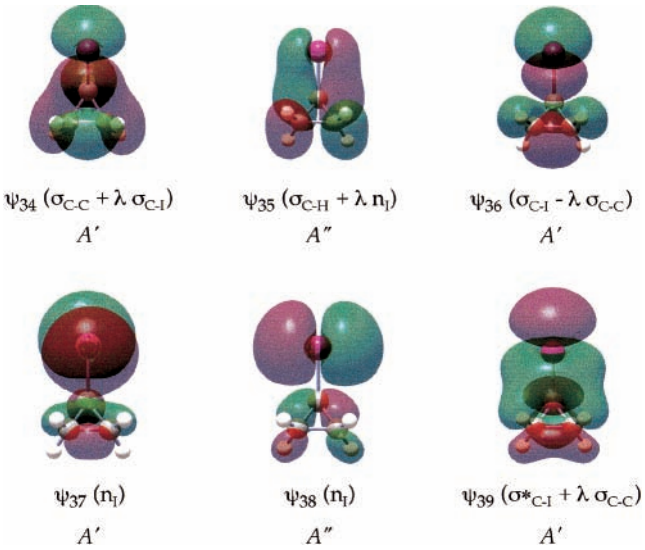

Figure 7. Molecular orbitals referred to in column 1 of Table 2. ψ_{38} is the HOMO and ψ_{39} is the LUMO of ground-state cyclopropyl iodide, according to the calculations.

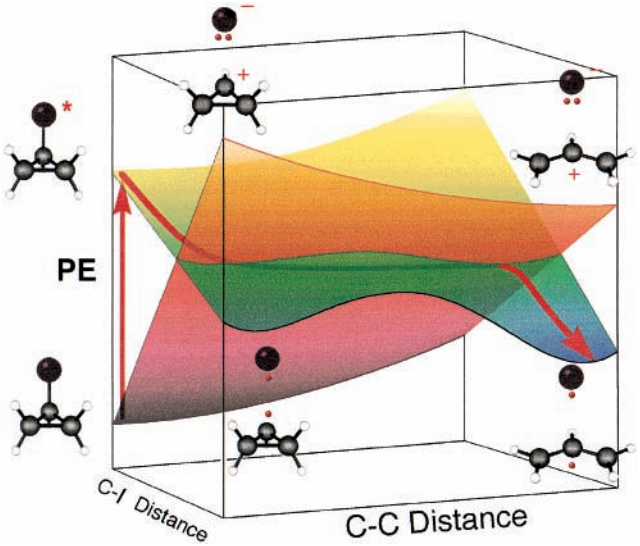

Figure 8. Schematic representation of a double surface-crossing mechanism for the direct formation of allyl radical and an iodine atom from photolysis of cyclopropyl iodide. The orange-red surface represents a closed-shell electronic state. The yellow-green-blue surface represents an open-shell singlet state, with the barrier to ring opening of the cyclopropyl radical depicted on the front face of the box. The red arrow shows the proposed path from the initially generated $^1(n,\sigma^*)$ excited state to the allyl radical and iodine atom products.

4.6. Intersections of Closed-Shell and Open-Shell Potential Energy Surfaces for Cyclopropyl Iodide. The experiments described above provide strong indications that there must be a *direct* pathway from the optically accessed electronic excited state of cyclopropyl iodide to allyl radical and an iodine atom. An appealing possibility would be that this pathway consists of two surface crossings. The first would be a crossing between the initially generated open-shell $^1(n,\sigma^*)$ state and a closed-shell ion-pair state. Several types of high-level ab initio theory have suggested that the cyclopropyl cation has no barrier to ring opening,[12] so the cyclopropyl cation/iodide ion pair would be expected to transform spontaneously to an allyl cation/iodide ion pair. A second surface crossing might then permit back electron transfer, with consequent generation of an allyl radical and an iodine atom. A double surface crossing of this kind would permit the system to sidestep the 22 kcal/mol barrier to adiabatic ring opening of the cyclopropyl radical.[10,11,42] The hypothetical mechanism is summarized schematically in Figure 8.

For this mechanism to be correct, it is a necessary condition that there exist (at least) two crossings between closed-shell and open-shell singlet states of the system. One crossing should occur at a long C−I distance but with a more-or-less normal distance of the C−C bond to be broken. The second should occur at a similar C−I distance but with a substantially elongated C−C bond. Two crossings that conform to these criteria have in fact been found by carrying out state-averaged CASSCF-(4,4) calculations, using the basis set described earlier.

The first crossing is a symmetry-allowed intersection of the A″ $^1(n,\sigma^*)$ state (corresponding to one of the two low-lying excited states of cyclopropyl iodide) and an A′ closed-shell state. The second corresponds to a same-symmetry conical intersection[43] between the A′ closed-shell state and an open-shell singlet A′ (σ,σ^*) state. The geometries of the lowest energy structures along these two seams of intersection are depicted in Figure 9. The orbitals involved in the CASSCF calculation and the principal configurations of each electronic state are summarized in Figures 10 and 11.

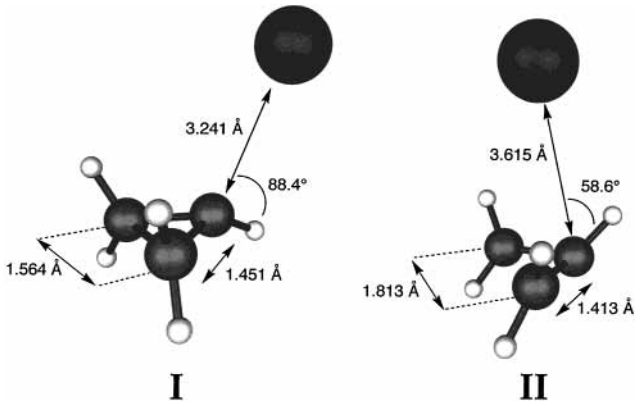

Figure 9. Geometries of the lowest energy points on the seams of intersection between the closed-shell surface and the A″ $^1(n,\sigma^*)$ (structure **I**) and between the closed-shell surface and the A′ $^1(\sigma,\sigma^*)$ surface (structure **II**).

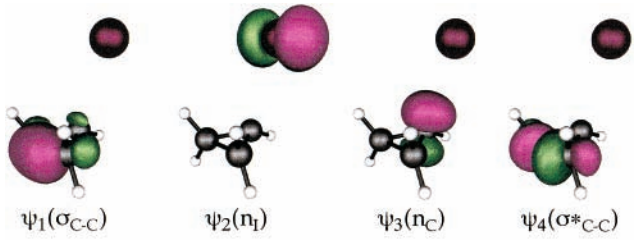

State 1: Energy = -7004.2821863892; SYM = A'

ALPHA SPIN				BETA SPIN				
ψ_1	ψ_2	ψ_3	ψ_4	ψ_1	ψ_2	ψ_3	ψ_4	COEFFICIENT
1	1	0	0	1	1	0	0	0.9907853
0	1	0	1	0	1	0	1	-0.1058010
1	1	0	0	0	1	1	0	0.0565287
0	1	1	0	1	1	0	0	0.0565287

State 2: Energy = -7004.2821861613; SYM = A"

ALPHA SPIN				BETA SPIN				
ψ_1	ψ_2	ψ_3	ψ_4	ψ_1	ψ_2	ψ_3	ψ_4	COEFFICIENT
1	1	0	0	1	0	1	0	0.6998877
1	0	1	0	1	1	0	0	0.6998877
0	1	0	1	0	0	1	1	-0.0770574
0	0	1	1	0	1	0	1	-0.0770574
0	1	1	0	1	0	1	0	-0.0632271
1	0	1	0	0	1	1	0	-0.0632271

Figure 10. Energy and principal configurations of the two states at the first crossing (structure **I** in Figure 9).

The first intersection corresponds closely to that anticipated in the schematic representation of Figure 8. However, the second does not. Rather than crossing back to the original A″ open-shell surface, this conical intersection connects the closed-shell surface with an A′ open-shell surface. Thus the diagram in Figure 8 really should have one closed-shell and two open-shell surfaces. However, we have retained the simpler representation both for purposes of visual clarity and also because the A′ and A″ open-shell singlet states must approach degeneracy as the C−I distance approaches infinity.

We have looked for an intersection between the closed shell state and the A′ open-shell state at the ring-closed geometry but have found none. Similarly, no crossing between closed-shell and A″ open-shell singlet states could be found with a ring-opened geometry. It is unclear whether the failure to locate these crossings derives merely from limitations of the calculations or whether the crossings really do not exist.

The calculations place the second intersection at an energy 5.8 kcal/mol above the first. However, the level of theory employed for the calculations is not sufficient for that to be considered a reliable figure. The system has substantial internal energy from the 266 nm (107.5 kcal/mol) photon that initiates

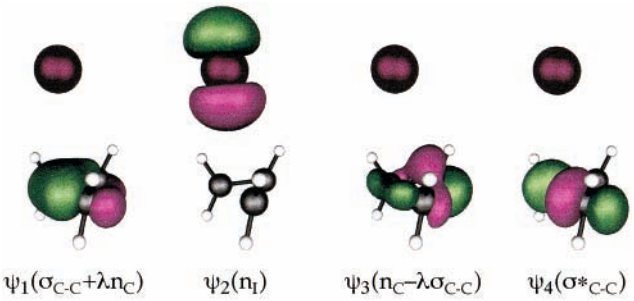

State 1: E = -7004.2729805617; SYM = A'

ALPHA SPIN				BETA SPIN				
ψ_1	ψ_2	ψ_3	ψ_4	ψ_1	ψ_2	ψ_3	ψ_4	COEFFICIENT
1	1	0	0	1	1	0	0	0.6414865
1	0	1	0	1	1	0	0	0.5026642
1	1	0	0	1	0	1	0	0.5026642
1	0	1	0	0	1	1	0	0.1499014
0	1	1	0	1	0	1	0	0.1499014
0	1	1	0	0	1	1	0	-0.1214528
0	0	1	1	0	1	0	1	-0.0762856
0	1	0	1	0	0	1	1	-0.0762856
0	1	0	1	0	1	0	1	-0.0646958
1	0	0	1	0	1	0	1	-0.0544118
0	1	0	1	1	0	0	1	-0.0544118

State 2: E = -7004.2729386279; SYM = A'

ALPHA SPIN				BETA SPIN				
ψ_1	ψ_2	ψ_3	ψ_4	ψ_1	ψ_2	ψ_3	ψ_4	COEFFICIENT
1	1	0	0	1	1	0	0	0.7372985
1	0	1	0	1	1	0	0	-0.4413127
1	1	0	0	1	0	1	0	-0.4413127
0	1	1	0	0	1	1	0	-0.1298028
1	0	1	0	0	1	1	0	-0.1123119
0	1	1	0	1	0	1	0	-0.1123119
0	1	0	1	0	1	0	1	-0.0774597
0	0	1	1	0	1	0	1	0.0684459
0	1	0	1	0	0	1	1	0.0684459
1	0	0	1	0	1	0	1	0.0644426
0	1	0	1	1	0	0	1	0.0644426

Figure 11. Energy and principal configurations of the two states at the second crossing (structure **II** in Figure 9).

the chemistry, and so a small rise in potential energy between the first crossing point and the second would presumably pose little problem for the reaction.

Both of the crossing points represent potential sites of bifurcation in the reaction dynamics. Some trajectories may choose to stay on the $^1(n,\sigma^*)$ surface at the first intersection. They would then form vibrationally excited cyclopropyl radical and an iodine atom. In solution, collisional cooling would almost certainly be faster than ring opening, and so this branch would lead to cyclopropyl-derived products. In the gas phase the hot cyclopropyl radical would open on a time scale of nanoseconds to the allyl radical.

For reactions in the gas phase or in inert solvents, trajectories choosing to stay on the closed-shell surface at the second crossing point could only reform the C−C and C−I bonds to return to cyclopropyl iodide. In a nucleophilic medium, interception of the cation by the solvent may be feasible. Such reactions are known in the photolysis of other alkyl halides.[1]

5. Conclusions

Experimental and computational evidence has been found for the existence of intersections between open-shell and closed-shell potential energy surfaces in the photodissociation of cyclopropyl iodide. In gas and solution phases, photoexcited cyclopropyl iodide appears to dissociate directly to form an iodine atom and an allyl radical. Ab initio calculations suggest that this occurs by way of two crossings between open-shell and closed-shell surfaces. The experiments show that the initially accessed electronic state of cyclopropyl iodide is of A′ symmetry. If the CASSCF calculations are correct, this state must undergo internal conversion to the A″ $^1(n,\sigma^*)$ state, which then experiences a symmetry-allowed intersection with the closed-shell ion-pair state. The cyclopropyl cation thus generated undergoes a barrierless ring opening to generate allyl cation. In a second surface crossing, allyl radical and an iodine atom are generated by a back electron transfer, occurring by way of a same-symmetry conical intersection. It is likely that such surface crossings are prevalent in alkyl halide photodissociations but can only be observed when the products from radical and ionic dissociation pathways differ. Continued studies will address the generality of this phenomenon.

Acknowledgment. This work was supported in part by the Department of Energy, Office of Basic Energy Sciences, under grants DE-FG01-88ER13934 and DE-FG02-98ER14857, and in part by the National Science Foundation, Division of Chemistry, under grant CHE-9901065.

References and Notes

(1) Kropp, P. J. *Acc. Chem. Res.* **1984**, *17*, 131.
(2) Szeimies, G.; Boche, G. *Angew. Chem., Int. Ed. Engl.* **1971**, *10*, 912.
(3) Dewar, M. J. S.; Kirschner, S. *J. Am. Chem. Soc.* **1971**, *93*, 4290.
(4) Farnell, L.; Richards, W. G. *J. Chem. Soc., Chem. Commun.* **1973**, 334.
(5) Merlet, P.; Peyerimhoff, S. D., Buenker, R. J.; Shih, S. *J. Am. Chem. Soc.* **1974**, *96*, 959.
(6) Dewar, M. J. S.; Kirschner, S. *J. Am. Chem. Soc.* **1974**, *96*, 5244.
(7) Beran, S.; Zahradnik, R. *Collect. Czech. Chem. Commun.* **1976**, *41*, 2303.
(8) Olivella, S.; Solé, A.; Bofill, J. M. *J. Am. Chem. Soc.* **1990**, *112*, 2160.
(9) Greig, G.; Thynne, J. C. J. *Trans. Faraday Soc.* **1966**, *62*, 3338.
(10) Greig, G.; Thynne, J. C. J. *Trans. Faraday Soc.* **1967**, *63*, 1369.
(11) Kerr, J. A.; Smith, A.; Trotman-Dickenson, A. F. *J. Chem. Soc. A* **1969**, 1400.
(12) Arnold, P. A.; Carpenter, B. K. *Chem. Phys. Lett.* **2000**, *328*, 90.
(13) DeFrees, D. J.; McIver, R. T., Jr.; Warren, J. H. *J. Am. Chem. Soc.* **1980**, *102*, 3334.
(14) Berkowitz, J.; Ellison, G. B.; Gutman, D. *J. Phys. Chem.* **1994**, *98*, 2744.
(15) Dupuis, M.; Pacansky, J. *J. Chem. Phys.* **1982**, *76*, 2511.
(16) Hudgens, J. W.; Dulcey, C. S. *J. Phys. Chem.* **1985**, *89*, 1505.
(17) NIST Webbook: http://webbook.nist.gov.
(18) Wilson, R. J.; Mueller, J. A.; Houston, P. L. *J. Phys. Chem. A* **1997**, *101*, 7593.
(19) Chang, B.-Y.; Hoetzlein, R. C.; Mueller, J. A.; Geiser, J. D.; Houston, P. L. *Rev. Sci. Instrum.* **1998**, *69*, 1665.
(20) Eppink, A. T. J. B.; Parker, D. H. *Rev. Sci. Instrum.* **1997**, *68*, 3477.
(21) Jung, Y.-J.; Kim, Y. S.; Kang, W. K.; Jung, K.-H. *J. Chem. Phys.* **1997**, *107*, 7187.
(22) Wang, D.; Li, Y.; Li, S.; Zhao, H. *Chem. Phys. Lett.* **1994**, *222*, 167.
(23) Frisch, M. J.; Trucks, G. W.; Schlegel, H. B.; Scuseria, G. E.; Robb, M. A.; Cheeseman, J. R.; Zakrzewski, V. G.; Montgomery, J. A., Jr.; Stratmann, R. E.; Burant, J. C.; Dapprich, S.; Millam, J. M.; Daniels, A. D.; Kudin, K. N.; Strain, M. C.; Farkas, O.; Tomasi, J.; Barone V.; Cossi, M.; Cammi, R.; Mennucci, B.; Pomelli, C.; Adamo, C.; Clifford, S.; Ochterski, J.; Petersson, G. A.; Ayala, P. Y.; Cui Q.; Morokuma, K.; Malick, D. K.; Rabuck, A. D.; Raghavachari, K.; Foresman, J. B.; Cioslowski, J.; Ortiz J. V.; Baboul, A. G.; Stefanov, B. B.; Liu G.; Liashenko, A.; Piskorz, P.; Komaromi, I.; Gomperts, R.; Martin, R. L.; Fox, D. J.; Keith, T.; Al-Laham, M. A.; Peng, C. Y.; Nanayakkara, A.; Gonzalez, C.; Challacombe, M.; Gill, P. M. W.; Johnson, B.; Chen, W.; Wong, M. W.; Andres, J. L.; Gonzalez C.; Head-Gordon, M.; Replogle, E. S.; Pople, J. A. *Gaussian 98 Rev. A.9;* Gaussian, Inc., Pittsburgh, PA, 1998.
(24) GAMESS (March 25, 2000 version for the Power Macintosh): Schmidt, M. W.; Baldridge, K. K.; Boatz, J. A.; Elbert, S. T.; Gordon, M. S.; Jensen, J. H.; Koseki, S.; Matsunaga, N.; Nguyen, K. A.; Su, S. J.; Windus, T. L. *J. Comput. Chem.* **1993**, *14*, 1347.
(25) Ragazos, I. N.; Robb, M. A.; Bernardi, F.; Olivucci, M. *Chem. Phys. Lett.* **1992**, *197*, 217.
(26) MacMolPlt 5.2.3: Bode, B. M.; Gordon, M. S. *J. Mol. Graphics Modell.* **1998**, *16*, 133.
(27) Castleman, K. R. *Digital Image Processing*; Prentice Hall, New York, 1996.
(28) Heck, A. J. R.; Chandler, D. W. *Annu. Rev. Phys. Chem.* **1995**, *45*, 335.

(29) Egger, K. W.; Cocks, A. T. *Helv. Chim. Acta* **1973**, *56*, 1516.
(30) Ferguson, K. C.; Whittle, E. *Trans. Faraday Soc.* **1971**, *67*, 2618.
(31) DePuy, C. H.; Gronert, S.; Barlow, S. E.; Bierbaum, V. M.; Damrauer, R. *J. Am. Chem.* Soc. **1989**, *111*, 1968.
(32) Seburg, R. A.; Squires, R. R. *Int. J. Mass Spectrom. Ion Proc*. **1997**, *167*, 541.
(33) 71.6 kcal/mol based on the heats of formation of isopropyl bromide (Davies, J.; Lacher, J. R.; Park, J. D. *Trans. Faraday Soc*. **1965**, *61*, 2413) and isopropyl radical (Tsang, W. In *Energetics of Organic Free Radicals;* Martinho Simoes, J. A., Greenberg, A., Liebman, J. F., Eds.; Blackie Academic and Professional: London, 1996; p 22.)
(34) 54.9 kcal/mol based on the heats of formation of isopropyl iodide (Furuyama, S.; Golden, D. M.; Benson, S. W. *J. Chem. Thermodyn*. **1969**, *1*, 363) and isopropyl radical (see ref 33).
(35) 80.7 kcal/mol based on the heats of formation cyclopropyl bromide (Holm, T. *J. Chem. Soc., Perkin Trans. 2* **1981**, 464. This paper reports $\Delta H_f°$ for liquid cyclopropyl bromide. The enthalpy of vaporization is apparently unknown, and so we have used Trouton's rule to estimate it from the boiling point. This approximation gives $\Delta H_{vap} = 7.2$ kcal/mol and $\Delta H_f° = 13.8$ kcal/mol for cyclopropyl bromide in the gas phase.) and cyclopropyl radical (see refs 31 and 32).
(36) 56.9 kcal/mol based on the heats of formation of methyl iodide (Cox, J. D.; Pilcher, G. *Thermochemistry of Organic and Organometallic Compounds*; Academic Press: New York, 1970) and methyl radical (Chase, M. W., Jr. *NIST-JANAF Themochemical Tables*, 4th ed.; *J. Phys. Chem. Ref. Data, Monograph 9*, 1998).
(37) Minsek, D. W.; Blush, J. A.; Chen, P. *J. Phys. Chem.* **1992**, *96*, 2025.
(38) Houle, F. A.; Beauchamp, J. L. *J. Am. Chem. Soc.* **1978**, 100, 3290.
(39) RRKMWSU by L. Zhu and W. L. Hase: Quantum Chemistry Program Exchange (Indiana University) #644.
(40) Newcomb, M. *Tetrahedron* **1993**, *49*, 1151 and references therein.
(41) Foresman, J. P.; Head-Gordon, M.; Pople, J. A.; Frisch, M. J. *J. Phys. Chem.* **1992**, *96*, 135.
(42) Walsh, R. *Int. J. Chem. Kinet.* **1970**, *2*, 71.
(43) Yarkony, D. R. *Acc. Chem. Res.* **1998**, *31*, 511.